PCCP

PAPER

View Article Online
View Journal | View Issue

Cite this: *Phys. Chem. Chem. Phys.*, 2025, **27**, 17910

Substituent effect on the excited state dynamics of bistable photochromic hydrazones

Maria Taddei,[a] Baihao Shao,[b] Bruce S. Lickey,[c] Qingkai Qi,[b] Matthew D. Liptak, *[c] Ivan Aprahamian *[b] and Mariangela Di Donato *[ad]

Received 25th March 2025,
Accepted 4th August 2025

DOI: 10.1039/d5cp01160d

rsc.li/pccp

Hydrazones are among the most promising newly developed photochromic molecules, often exhibiting very high isomerization quantum yields, long and tunable half-lives and excellent photostability. It has recently been demonstrated that substitutions on the hydrazone core with electron donating (EDG) or withdrawing (EWG) groups on either the rotor or stator moiety can greatly influence their photoswitching properties, in some cases conferring new and interesting properties onto them, such as emission toggling and two-photon activity. Here, we analyze the photodynamic behavior of three representative substituted hydrazones in depth, using ultrafast visible and infrared transient absorption spectroscopies, and perform density functional theory calculations to interpret their steady-state spectra. In particular, we focus on systems having an EDG and/or EWG substituent on the stator and rotor moieties, whose principal effect is to red shift the absorption spectra of the *Z* and *E* isomers relative to the parent unsubstituted hydrazone. Our results highlight the effect that substituents have on the isomerization and emission mechanisms of the hydrazones, and subsequently on their spectroscopic properties. Moreover, these studies elaborate on how the substituents and solvent polarity play important roles in altering the isomerization quantum yield.

Introduction

Photochromic compounds that respond to light absorption through a variation of their conformational, chemical or physical properties[1] can be applicable in many different fields, spanning from the production of responsive materials and surfaces,[2,3] to energy conversion,[4–6] catalysis,[7] drug delivery,[8,9] design of molecular machines,[10–13] super resolution microscopy[14,15] and the biomedical field.[16–19] To date, numerous classes of photoswitches have been developed and applied, with azobenzenes,[20] spiropyranes[21] and diarylethenes[22] being among the most widespread. The quest for switches with optimized properties has promoted a surge of research activity focussed on developing new molecules and improving their properties, such as quantum yields (QYs), photostability, thermal relaxation half-lives ($\tau_{1/2}$), fatigue resistance and activation wavelengths.

A major breakthrough in this area came from the development of a new family of bistable hydrazone switches, having outstanding $\tau_{1/2}$ as long as 5000 years.[23] These molecules combine many of the desired properties of photochromic systems and have been successfully applied in controlling the self-assembly of liquid crystals and inducing opto-mechanical properties in polymers, among other applications.[24–28] Bistable hydrazones, having phenyl rings both at the stator and rotor parts (Scheme 1), can be easily synthesized and derivatized, opening the way for the straightforward modification of their switching properties to match desired applications. For instance, quite recently it was discovered that the introduction of a *para*-dimethyl amine substituent (NMe_2) on the rotor phenyl moiety makes the *Z* isomer of this compound highly fluorescent both in solution and the solid state, with luminescence that can be turned OFF upon isomerization to the *E* form.[29] Following this initial study, several compounds were synthesized to study the effect of introducing electron withdrawing or electron donating groups (EWG and EDG, respectively) on the rotor or stator phenyl rings.[30] It was realized that the properties of these hydrazones, in terms of $\tau_{1/2}$, isomerization QYs, photostationary states (PSSs) and fluorescence both in solution and the solid state are greatly influenced by the nature of the substituents on the phenyl rings. For instance, it was found that substituting NO_2 either at the stator or rotor moieties induces a substantial red shift of the absorption maxima of the *Z* isomer. In the former case it is because of an extension of the π-system through resonance between the NO_2 group and the hydrazone

[a] *LENS – European Laboratory for Non-linear Spectroscopy, via N. Carrara 1, 50019 Sesto Fiorentino (FI), Italy. E-mail: didonato@lens.unifi.it*
[b] *Department of Chemistry, 6128 Burke Laboratory, Dartmouth College, Hanover, New Hampshire 03755, USA. E-mail: ivan.aprahamian@dartmouth.edu*
[c] *Department of Chemistry, University of Vermont, Burlington, Vermont 05405, USA. E-mail: Matthew.Liptak@uvm.edu*
[d] *CNR-ICCOM, via Madonna del Piano 10, 50019 Sesto Fiorentino (FI), Italy*

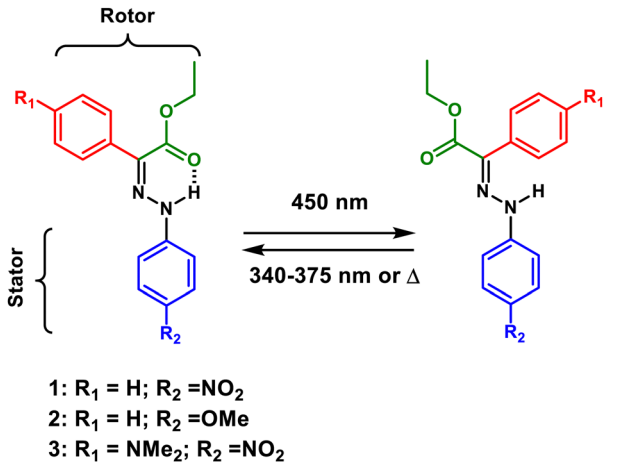

Scheme 1 Light-induced *E*/*Z* isomerization of the three hydrazone photoswitches used in this study. The stator moiety (arbitrary designation) is depicted in blue, while the rotor moiety is shown in red and green colours.

amino nitrogen, while in the latter case it is because of a LUMO stabilization effect.[30]

In general, EDG substituents both on the rotor and stator moieties induce a red shift in the absorption and emission spectra of the more stable *Z* isomers, while the effect on the isomerization $\tau_{1/2}$, PSS and fluorescence properties can vary, depending on the chemical nature of the appendant. To correlate the effect of different substituents with the photoswitching activity, an in-depth steady state spectroscopic characterization of ten differently substituted hydrazones was previously performed,[30] which rationalized most of the observed properties. Nevertheless, several open questions remain: for example, the influence of the different substituents on the photoswitching mechanism and the excited state dynamics of these hydrazone switches have yet to be investigated. It has been previously suggested that the fluorescence in these systems may arise from charge transfer (CT) and excited state proton transfer, while a recent theoretical investigation suggests that H-bond rigidification might be the actual culprit.[31] Furthermore, all of the previous studies were conducted in toluene (TOL),[30] and the effect of solvent polarity, which in principle could greatly affect the photodynamics of these systems, was not investigated.

A clear understanding of the structure–function relationships of molecular photoswitches is essential to engineer systems with properties that could be specifically addressed for different applications. In this particular case, a deep understanding of the influence of EDGs or EWGs on the photoswitching mechanism of the hydrazones is mandatory to design new molecules with improved properties and predictable light-induced operation. To reach this goal, we applied transient absorption spectroscopy with sub-picosecond time resolution both in the visible and infrared (IR) spectral ranges on three representative systems selected within the series of the ten compounds previously presented.[30] The three targeted compounds—**1**, having a NO_2 substituent on the stator phenyl ring, **2**, having an OMe group at the stator phenyl ring, and the push–pull system **3**, which has a NO_2 group at the stator phenyl ring and a NMe_2 group on the rotor phenyl moiety (Scheme 1) making it fully addressable with visible light[30]—were specifically selected because they would allow us to obtain a broad understanding of the effects of EWGs and EDGs and their substitution pattern on the properties of hydrazone switches, without having to characterize a whole ensemble of molecules.

We also considered how the polarity of the solvent influences the photoswitching abilities of these compounds and complemented the spectroscopic characterization with a theoretical analysis based on density functional theory (DFT) computations, which helped in the interpretation of the experimental outcomes. The joint analysis of our experimental and theoretical results provides new insights into the influence of diverse molecular substituents on the photoswitching properties of the hydrazone compounds, enabling an in-depth rationalization of the structure–function relationship of this class of photochromic molecules.

Experimental

Transient absorption spectroscopy

The apparatus used for the transient absorption spectroscopy (TAS) measurements is based on a Ti:sapphire regenerative amplifier (Amplitude Pulsar) system pumped by a home-made Ti:sapphire oscillator. The system produces 100 fs pulses at 785 nm, 1 kHz repetition rate and average power of 450–500 mW. Excitation pulses at 400 nm have been obtained by second harmonic generation of the fundamental laser output, while pulses at 450 nm have been obtained by frequency mixing on a BBO crystal a small portion of the fundamental laser output and the near-IR signal output of a TOPAS (Light Conversion) Optical Parametric Amplifier (OPA). The pump beam polarization has been set to magic angle with respect to the probe beam by rotating a $\lambda/2$ plate. Excitation powers were on the order of 100–150 nJ. The probe pulse was generated by focusing a small portion of the fundamental laser output radiation on a 3 mm thick calcium fluoride window. Pump–probe delays were introduced by sending the probe beam through a motorized stage. Multichannel detection was achieved by sending the white light continuum, after passing through the sample, to a flat field monochromator coupled to a home-made CCD detector. TAS measurements were carried out in a quartz cell (2 mm thick) mounted on a movable stage to avoid sample photo degradation and multiple photon excitation. The time resolution of the experiment is of about 150 fs. Data have been acquired in a time interval spanning up to 1.5 ns for long living samples. The transient spectra of samples decaying on a shorter timescale have been acquired up to 300 ps. For transient IR measurement a different a Ti:sapphire regenerative amplifier and Ti:sapphire oscillator were used (respectively Coherent Legend Elite amplifier and Coherent Micra Oscillator). The system delivers 40 fs pulses at 800 nm, 1 kHz repetition rate and 3 W power. The visible pump pulses

have been obtained either by second harmonic generation of the fundamental laser output within a 2 mm thick BBO crystal (400 nm), or by frequency mixing on a BBO crystal the signal output of obtained from an optical parametric amplifier (TOPAS, Light Conversion) with the residual 800 nm beam entering the OPA (pulses at 450 nm). The probe beam in the mid-IR is obtained through difference frequency mixing of the near IR signal and idler output generated from a home-made optical parametric amplifier. Multichannel detection is obtained by sending the probe beam, after crossing the sample, through a monochromator coupled to a nitrogen cooled MCT detector (Infrared Associated). Pump–probe delay are introduced by sending the pump beam though a motorized delay stage. The sample was contained in a demountable cell composed by two calcium fluoride windows separated by a 50 μm Teflon spacer. The cell was mounted on a movable sample holder to avoid sample photodegradation, multiple excitations and minimize the accumulation of the photogenerated isomers. The time resolution of the experiment is of about 200 fs. Data have been acquired in a time interval spanning up to 1 ns for long living samples. The transient spectra of samples decaying on a shorter timescale have been acquired up to 300 ps. The recorded kinetic traces and transient spectra both in the visible and MidIR have been analysed by using a global analysis procedure.[32] The number of kinetic components has been estimated by performing a preliminary singular values decomposition (SVD) analysis,[33] Global analysis was performed using the GLOTARAN package (**https://glotaran.org**),[34] and employing a linear unidirectional "sequential" model. Sample concentration used for visible transient absorption measurements were about 2.5×10^{-4} M. For Visible-pump/MidIR-probe measurements samples concentrations were approximately 10^{-3} M.

Time correlated single photon counting (TCSPC)

The fluorescence lifetimes were determined by time-correlated single photon-counting (TCSPC) using a Photon Technology International S4 QuantaMaster 4 spectrofluorometer integrated with Deltadiode-375L diode laser (λ_{ex} = 373 nm, <70 ps pulse width) as the excitation source. The fluorescence decays were detected using a fast PPD-850 detector. In all cases, decays were recorded until peak counts reached 10 000. The decay traces were analyzed by the single exponential fitting method using Felix data analysis from Horiba Scientific Ltd.

DFT and TDDFT computations

The geometries of both the *E*- and *Z*-isomers of compounds **1**, **2**, and **3** were optimized using density functional theory as implemented within the ORCA 5.0.4 software package.[35–37] These optimized structures were then used to compute the simulated IR spectra through a DFT analytical frequency calculation. Both the optimization and frequency calculations were performed using the PBE0 hybrid functional with the def2-TZVP basis set and def2-J auxiliary basis set, as well as the "VeryTightSCF" keyword.[38,39] Solvated systems were modelled using the conductor-like polarizable continuum model (CPCM) of solvation during both structural optimization and spectral simulation.[40]

TDDFT predictions of the UV-Vis absorption and fluorescence spectra of compound **3** were computed using the same basis sets as above but used the ωB97x functional[41] and the ORCA 5.0.1 software package instead, following a series of preliminary test calculations on compound **3** in DCM at varying levels of theory (Fig. S22).[42] Solvated systems were modelled using the conductor-like polarizable continuum model (CPCM) of solvation during both structural optimization and spectral simulation.[40] Ground-state (S_0) geometries were re-optimized *via* DFT for each solvent system at this level of theory prior to TDDFT treatment for computing the UV-Vis absorption spectra. The resulting output was then used to obtain excited state geometries by performing TDDFT optimizations at the computed S_1 state, followed by a similar TDDFT treatment of this geometry to calculate the emission spectra. All ORCA 5 input files used the "VeryTightSCF" keyword, with the TDDFT computations being performed under the Tamm–Dancoff approximation with the "NRoots" flag set to 100 and the "MaxDim" flag set to 6. Spectra were simulated by convoluting Gaussian-shaped bands with linewidths of 4700 cm^{-1} centered around each spectral line with intensities derived from the oscillator strength of each transition.

Molecular orbital and electron density difference plots were calculated from the TDDFT outputs *via* the orca_plot program, which were used to generate isosurfaces using VMD 1.9.3[43] and rendered in Blender 4.2.

DFT and TDDFT calculations were performed in part on the Vermont advanced computing core.

Synthesis

Compounds **1**, **2**, and **3** (Scheme 1) were synthesised using a previously reported procedure.[25,30] Upon light absorption they undergo isomerization around the imine C=N bond, converting from the stable *Z* to the "metastable" *E* form.

Results and discussion

Steady state spectroscopy and DFT computations

The spectroscopic properties of compounds **1**, **2** and **3** have been previously studied in fine-details in toluene, revealing strikingly different behaviour in terms of isomerization QYs, PSSs and $\tau_{1/2}$.[30] Based on our findings, the emission efficiency of the *Z* isomers of compounds **1** and **2** in all solvents is quite low, and a reliable emission QY cannot be measured. While the *Z*-isomer of compound **3** has a fluorescence QY of about 22% in TOL, its emission efficiency in moderately polar to polar solvents drastically decreases, again preventing reliable fluorescence QY estimation. Each of the *E* isomers are practically non-emissive.[30] Previously it was found that compound **1** has very high PSSs for both the forward (PSS_{442} = 98% *E*) and reverse (PSS_{365} = 82% *Z*) isomerization processes and good QY for the *Z*/*E* isomerization in toluene ($\Phi_{Z\rightarrow E}$ = 35.3%; $\Phi_{E\rightarrow Z}$ = 11.4%) with $\tau_{1/2}$ amounting to 1286 years for the $E \rightarrow Z$ thermal isomerization process.[30] Very high PSS values (PSS_{442} = 93% *E*; PSS_{340} = 88% *Z*) but moderate photoisomerization quantum

yields ($\Phi_{Z\rightarrow E}$ = 5.3% and $\Phi_{E\rightarrow Z}$ = 9.5%) and shorter $\tau_{1/2}$ of tens of days characterize compound **2**. This behaviour has been rationalized by considering that the addition of an EDG to the stator phenyl ring enhances the conjugation within the molecule, reducing the double bond character of the imine C=N bond and thus the energy barrier for the thermal relaxation process. The best performance was recorded for compound **3**, for which visible light can be used to switch the molecule in both directions with great PSSs (PSS_{480} = >99% *E*; PSS_{375} = 96% *Z*; PSS_{410} = 90% *Z*). This compound also presents a good QY for the isomerization ($\Phi_{Z\rightarrow E}$ = 46.2% and $\Phi_{E\rightarrow Z}$ = 7.4%) and a $\tau_{1/2}$ of 126 years.[20,30]

Because the polarity of the external medium can greatly influence the photoswitching properties of these compounds, particularly in the case of the push–pull compound **3**, we repeated all our spectroscopic measurements in three solvents with different polarities, namely TOL, dichloromethane (DCM) and acetonitrile (ACN). Fig. 1 reports the absorption and fluorescence spectra of the compounds in these three solvents. Excitation spectra at different emission wavelengths were measured for compound **1** in TOL, DCM and ACN (Fig. S1) while its emission lifetimes were found to be shorter than the time resolution of the single photon counting setup. Compound **2** has a very low fluorescence QY in all solvents, but to exclude the presence of impurities, an excitation spectrum has been measured in ACN (Fig. S2c). We also measured the excitation spectra for compound **3** at different emission wavelengths in TOL and its emission lifetime (2.7 ns), which could be fitted with a single exponential function (Fig. S2b). Excitation spectra and emission lifetimes of **3** could not be measured in DCM nor ACN because of the very low fluorescence intensities. The excitation spectra of all samples remained the same, independent of the monitored emission wavelength, confirming the absence of any fluorescent impurities.

As seen in Fig. 1a, the absorption spectra of compound **1** in the three solvents are very similar. They present an intense band centered at about 390 nm, which only slightly red shifts in DCM. In contrast, the emission spectra are influenced by solvent polarity. The emission maximum in toluene (blue dashed line) is at 455 nm, and red shifts by 49 and 73 nm in DCM and ACN, respectively. The observed strong influence of solvent polarity suggests that the emissive state has a CT nature.

In the case of compound **2**, the absorption spectra (Fig. 1b) present an intense band centered around 380 nm in TOL, which shows a progressively limited blue-shift with increasing solvent polarity. The effect of solvent polarity on the fluorescence band is also not pronounced, nevertheless the emission maximum red shifts by nearly 20 nm in both DCM and ACN as compared to that in TOL.

Finally, the absorption spectra of compound **3** (Fig. 1c) shows minimal solvent dependence, featuring a 434 nm band that slightly red shifts in DCM and slightly blue shifts in ACN relative to TOL. The emission spectra exhibit a similarly minor spread, ranging from 535 to 547 nm; nevertheless, their intensities in polar solvents are substantially reduced relative to TOL (see *infra*). The result is a relatively consistent range of Stokes shifts (between 0.5 and 0.6 eV) among the three solvent

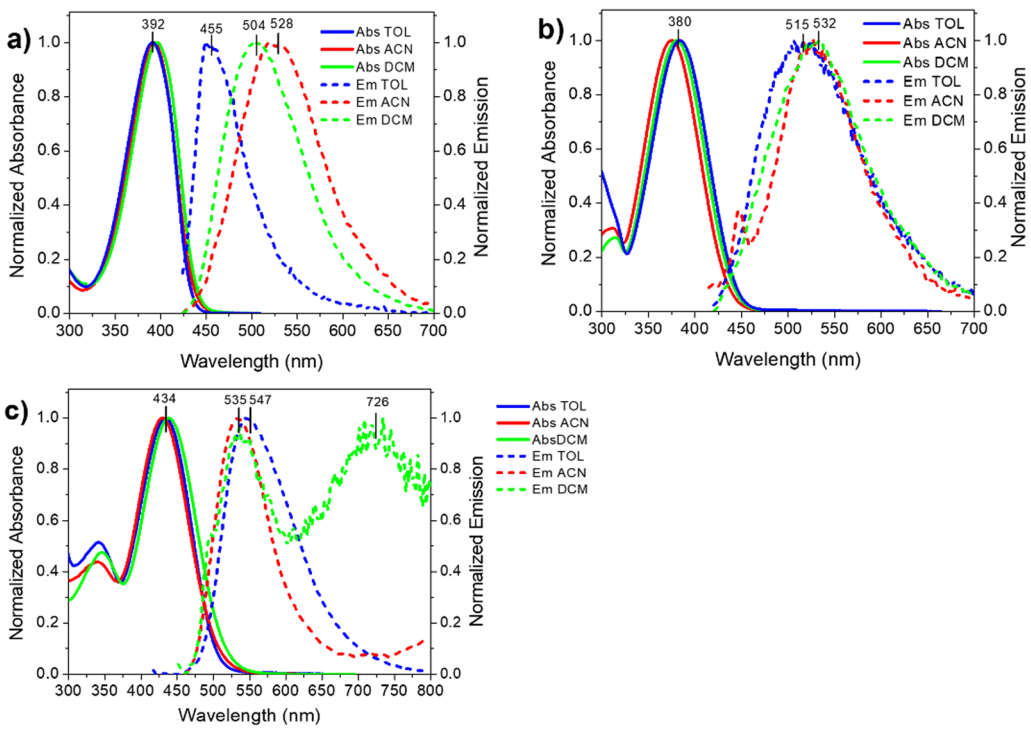

Fig. 1 Absorption (solid lines) and emission (dashed lines) spectra of the *Z* isomers of compounds **1** (a), **2** (b) and **3** (c) in TOL (blue line), ACN (red line) and DCM (green line).

systems. Additionally, the emission in DCM exhibits a red-shifted secondary peak centered around 730 nm; repeated measurements at varying concentrations suggest aggregation or excimer formation as a potential origin for this band, since its intensity increases with concentration (Fig. S3). Lastly, the emission in ACN exhibits a low intensity tail which is absent in TOL.

As mentioned previously, the emission of compound **3** is highly quenched in polar solvents compared to TOL. This behavior is quite typical for molecules emitting from an excited state presenting a CT character, which is greatly stabilized in polar environments, as expected in the case of the push–pull hydrazone **3**.

To further assess the presence of a CT state, UV/Vis absorption and emission spectra were computed for compound **3** in DCM, TOL, ACN, and in the gas-phase using time-dependent DFT (TDDFT) with CPCM solvation (Fig. 2). The choice of functional was made by surveying varying levels of theory, using DCM solvation as a model for comparison with the experimental UV/Vis absorption spectra of compound **3** in this solvent. These included the GGA functional PBE,[44] hybrid functionals PBE0[44] and B3LYP,[45–47] long-range corrected hybrid functionals ωB97 and ωB97X,[48] and the long-range corrected double-hybrid functional ωB2GP-PLYP.[49] TDDFT results using the GGA and hybrid functionals predicted broad, red-shifted absorption bands that were absent from the experimental spectra, as well as being weaker in intensity relative to higher-energy transitions. The long-range corrected functionals, however, did not predict such features, and produced relative intensities between peaks that were more closely aligned with experimental results. While the absolute energy of the S_1 transition calculated using the double-hybrid ωB2GP-PLYP[49] functional was nearest to that of the experimental maximum at 434 nm, ωB97X was ultimately chosen for further TDDFT of compound **3** as it provided relatively comparable results for substantially lower computational costs (see Fig. S25 for details).

Much like what was observed experimentally, the absolute energies of the first absorption band exhibit minimal solvent dependency among the computed spectra, with a range of less than 0.02 eV among all three simulated solvent conditions. These transitions correspond to the absorbance maxima centered at approximately 430 nm in the experimental spectra seen in Fig. 1c.

A shortcoming with the use of TDDFT is that the absolute energies of computed transitions are typically shifted relative to their experimental values; this occurs as a consequence of using the electronic ground state orbitals to describe the electronic excited state. Here, the experimental absorbance maxima occurred in the range of approximately 430 nm, whereas the TDDFT predictions generally occurred near 340 nm, with the closest result occurring near 400 nm when using the long-range corrected double hybrid functional ωB2GP-PLYP. Hence, the Stokes shifts between the lowest-lying absorbance and emission bands present a more meaningful method of comparing the TDDFT results to experiments. The average discrepancy of around 0.3 eV between the experimental and TDDFT Stokes shifts is similar in magnitude to the variation in peak positions observed during initial testing of the choice of functional and aligns with typical deviations from experiment for TDDFT-predicted electronic spectra.

The TDDFT-computed fluorescence spectra of compound **3** appeared to red-shift slightly with increasing solvent polarity. This trend is in turn reflected by the Stokes shifts (which were 0.81, 0.83, and 0.86 eV for TOL, DCM, and ACN, respectively), becuase of the negligible polarity dependence of the absorption maxima. While this trend opposes the blue-shifting that was observed experimentally, the 0.06 eV range in Stokes magnitudes across all three solvent systems closely mirrors the experimental distribution. Furthermore, it should be noted that oscillator strengths for the $S_1 \rightarrow S_0$ transition calculated *via* TDDFT are not reflective of the overall fluorescence intensities; such a model would not be possible without also accounting for the dynamics of competing nonradiative pathways across solvent systems, which in this case are likely to be driven by differences in vibrational relaxation processes as evidenced by transient IR data (*vide infra*). Lastly, as the

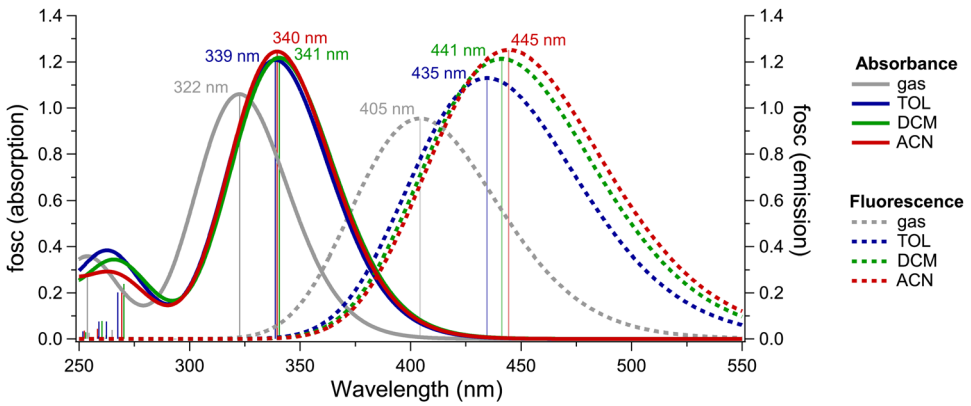

Fig. 2 TDDFT-predicted UV/Vis absorption (solid lines) and emission (dashed lines) spectra for the *Z* isomer of compound **3** in the gas-phase, TOL, ACN, and DCM. Dark and light vertical lines represent the individual calculated transitions for the absorbance and fluorescence spectra, respectively. All DFT and TDDFT calculations were performed at the ωB97X/def2-TZVP level of theory, with CPCM solvation where applicable.

simulated data only represent theoretical single-molecule spectra, the lack of a secondary redshifted feature in the computed DCM emission spectrum supports the possibility of this feature originating from the formation of aggregates or excimers.[30]

In addition to the simulated electronic spectra, the TDDFT data also provide theoretical descriptions for the excited state distortion and the molecular orbitals involved in the excitation and emission processes. With regards to the structural change in the excited state following photoexcitation, three notable changes were observed. The hydrogen bond length decreased by 0.12 to 0.14 Å, the C–N bond connecting the rotor and stator increases by 0.06 to 0.07 Å, and the C–C bond connecting the rotor phenyl to the imine carbon decreases by 0.03 to 0.05 Å. With regards to the molecular orbitals involved the electronic transitions, their properties support a CT description of the chromophore. As shown in the electron density difference plot (EDDP) in Fig. 3, the $S_0 \rightarrow S_1$ transition in compound **3** exhibits a clear push–pull redistribution of charge density that decreases near the rotor moiety containing an electron donating NMe_2 group and increases towards the stator moiety containing an electron withdrawing NO_2 group as suggested. The results also characterize the distinct orbital pairs involved in this transition and demonstrate that the primary contribution is between a HOMO localized on the rotor and a LUMO localized on the stator. However, a detailed examination of the EDDP reveals that the electronic transition is not a pure CT transition, as there is some electron donation from the stator back to the rotor. Several groups have developed tools to quantify the CT nature of a TDDFT transition,[50–53] and a fragment-based approach *via* the program TheoDORE was employed here (Fig. 4).[54,55] The $S_0 \rightarrow S_1$ excitation of **3** had a CT number of 0.6 (Fig. 4c), which describes a transition with moderate CT character. The CT number increases slightly following excited state relaxation, approaching 0.7 for the $S_1 \rightarrow S_0$ emission.

We then measured the FTIR spectra of the *Z* isomers of the samples in DCM, which are reported in Fig. 5. Assignments of the most intense vibrational bands are based on DFT computations performed at the PBE0/def2-TZVP level of theory. The spectra obtained from DFT computations for the *Z* isomers in DCM are reported in the same figure, for comparison with the experimental spectra.

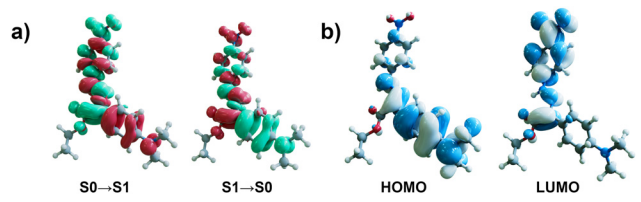

Fig. 3 (a) Electron density difference plots for the $S_0 \rightarrow S_1$ and $S_1 \rightarrow S_0$ transitions in compound **3** in acetonitrile. Red lobes indicate a net decrease in the local electron density, while green indicates an increase. (b) Dominant contributing orbitals (left, HOMO; right, LUMO) for the $S_0 \rightarrow S_1$ transition. Analogous plots for the remaining solvent systems can be found in Fig. S24.

The spectra of compounds **1** and **3** recorded in the 1200–1800 cm^{-1} region are quite similar, while some difference is noted for compound **2**. The C=O stretching mode in all compounds is experimentally observed to absorb in the 1680–1700 cm^{-1} region. Calculations underestimate the C=O frequencies, which are predicted at about 1640 cm^{-1}, possibly because they overestimate the strength of the H-bond between the carbonyl and the NH group. Based on computations, the intense band observed at 1600 cm^{-1} for both compound **1** and **3** can be assigned to the aromatic C=C stretching, while the double peak experimentally observed at 1510–1534 cm^{-1} is assigned to a delocalized mode involving the C=N, N–N, and N–H stretching. According to calculations, in the case of compound **3** the most intense contribution from the C=N stretching is at 1502 cm^{-1}. The band experimentally observed at 1335 cm^{-1} can be assigned to the NO_2 stretching mode, with the corresponding computed frequency being at 1280 cm^{-1}. Bands below 1200 cm^{-1} mostly arise from the ester C–O stretching and C–H and C–N bending modes. Mode assignments for compound **2** are quite similar aside from the obvious lack of an NO_2 stretch. For this compound bands at 1500–1530 cm^{-1} mostly arise from aromatic C=C stretching vibrations of the rotor and stator moieties, with a small contribution from the C=N stretching. The C=N and N–N stretching vibrations mostly contribute to a normal mode computed at 1508 cm^{-1}, which has however low oscillator strength. The only other normal mode with appreciable oscillator strength, bearing contributions from the C=N and N–N stretching is quite delocalized, and involves also the aromatic rotor and stator moieties. Its frequency is computed at 1442 cm^{-1}. Modes of the –OMe substituent are mixed with those of the aromatic rings and are mostly found in the 1200–1300 cm^{-1} region.

Transient absorption spectroscopy

The excited state dynamics of the three substituted hydrazones has been studied by measuring their ultrafast pump–probe spectra. The excitation wavelength has been set at 400 nm for compounds **1** and **2**, while compound **3** was excited at 450 nm to avoid back excitation of the *E* isomer. As for the steady state spectra, measurements were repeated in ACN, DCM, and TOL. The kinetic constants describing the dynamics of excited state relaxation have been extracted using global analysis and applying a linear unidirectional decay scheme. This kinetic scheme is useful to extract the overall kinetic constants describing the excited state evolution but does not retrieve the 'pure' spectra of the different species formed upon photoexcitation. The number of kinetic components necessary for a satisfactory global fit has been determined by performing a preliminary singular value decomposition (SVD) analysis.

The evolution associated difference spectra (EADS) obtained analysing the data measured in TOL for the three samples are shown in Fig. 6. The experimental raw data, selected kinetic traces, and additional EADS are reported in the SI (Fig. S4–S15).

As noticed from Fig. 6, the excited state behaviour of the three compounds is markedly different.

For compound **1**, the transient spectra recorded at early delay times present an intense and broad positive excited state

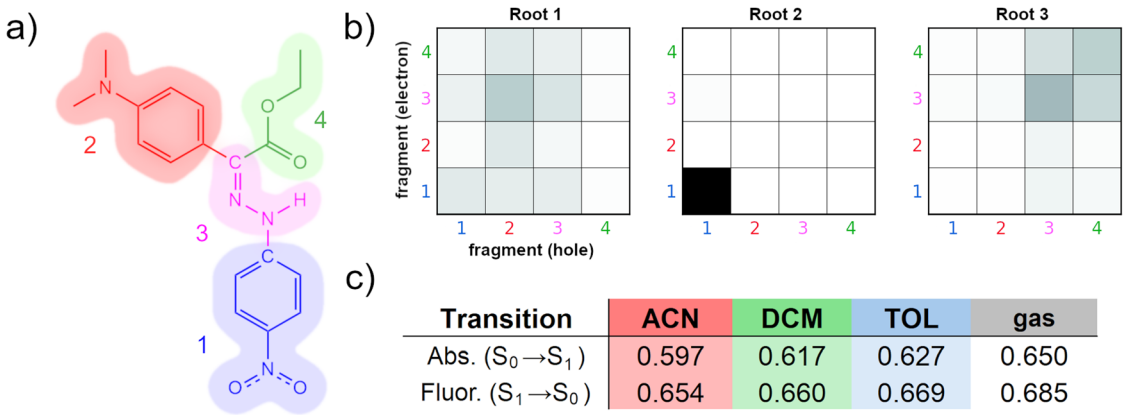

Transition	ACN	DCM	TOL	gas
Abs. ($S_0 \rightarrow S_1$)	0.597	0.617	0.627	0.650
Fluor. ($S_1 \rightarrow S_0$)	0.654	0.660	0.669	0.685

Fig. 4 (a) Molecular fragment definitions used for the CT analysis of TDDFT results for the *Z*-isomer of **3**. (b) Ω-Matrix plots for the first three roots from the S_1 TDDFT of **3**(*Z*) in ACN. Additional plots for both S_0 and S_1 in each solvent system can be found in Fig. S26. Off-diagonal elements reflect cross-fragment electron–hole separation, while the degree of asymmetry of these elements across the diagonal corresponds to a net CT across the molecule. Roots **2** and **3** are included as counterexamples reflecting minimal CT character. (c) Calculated CT numbers for the $S_0 \rightarrow S_1$ and $S_1 \rightarrow S_0$ transitions in each solvent system, defined as the normalized sum of inter-fragment CT amplitudes.

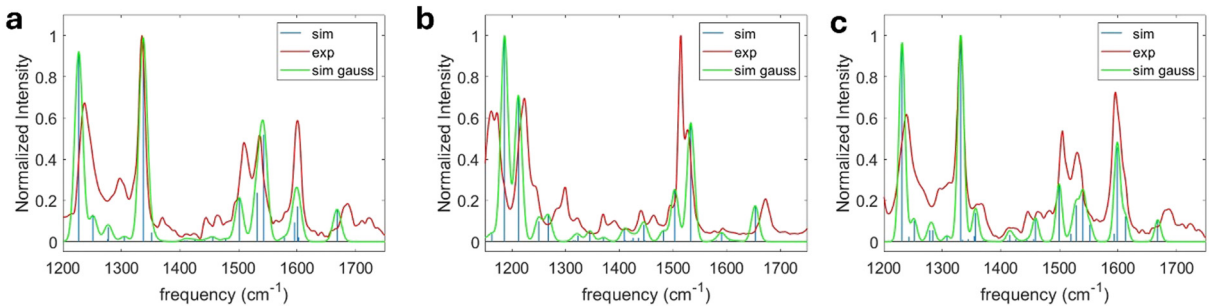

Fig. 5 FTIR spectra of the *Z* isomers of compounds **1** (a), **2** (b), and **3** (c) recorded in DCM, and comparison with the respective computed IR spectra obtained at PBE0/def2-TZVP level. To obtain the computed IR spectra, the calculated intensities have been convoluted with Gaussian functions with 8 cm^{-1} FWHM; a scaling factor of 0.96 has been applied to the computed frequencies to better match the experimental ones. The computed spectra have been generated using a MATLAB script.

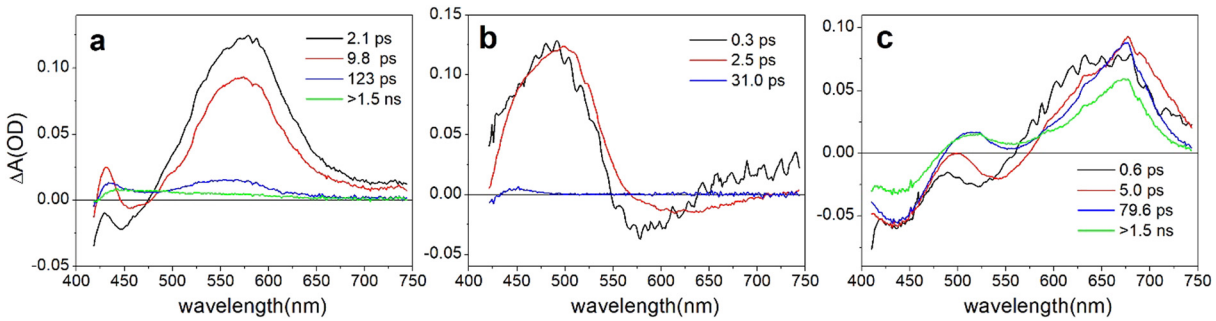

Fig. 6 EADS obtained from global analysis of the transient data recorded by exciting the *Z* isomer of compound (a) **1**; (b) **2**; (c) **3** in TOL.

absorption (ESA) band centred at 570 nm. A negative stimulated emission (SE) band is also observed, peaked at 450 nm, whose position agrees with the steady state fluorescence recorded for its *Z* isomer (Fig. 1a). The ground state bleaching (GSB) band is not visible, being outside the recorded spectral interval. The transient spectra of the other two compounds appear different: compound **2** indeed presents an ESA peaked at about 480 nm and a SE band at 570 nm, which rapidly red shifts and broadens within a few hundred femtoseconds. For compound **3**, presenting a red-shifted ground state absorption, both GSB and SE are visible in the transient spectra, peaking respectively at 440 and 525 nm. Furthermore, and intense and broad ESA is present, peaking at 670 nm.

All compounds undergo spectral changes on a fast timescale of 1–2 ps, reflecting rapid relaxation processes induced by the solvent response. The spectral evolution involves in all cases

minor shifts and decreases in intensity of the ESA bands and a red shift of the SE bands, associated with excited state relaxation.

The dynamic evolution on the longer timescale is instead substantially different for the three samples.

For compound **1**, both the ESA band centred at 570 nm as well as the SE band decay almost completely within 9.8 ps. It is known from previous studies[30] that compound **1** has a good $Z \rightarrow E$ photo-isomerization QY in toluene of about 35%. From the data in Fig. 6a we infer that isomerization occurs within the timescale associated to the excited state decay, thus about 10 ps, signalled by the decay of the ESA band peaking at 570 nm. The broad and low intensity signal observed in the third EADS can be assigned to the absorption tail of a hot ground state population of the photoproducts, since the molecules reach the ground state quite rapidly and with an excess of energy. The further evolution occurring within 18.8 ps, is interpreted as the cooling of the hot ground state. The long living final EADS should represent the absorption tail of the isomerization product, but the maximum absorption of the *E* isomer is in the UV range,[30] not directly accessible within the investigated spectral range. Since both the bleaching signal of the *Z* isomer and the main product band of the *E* isomer are out of the investigated spectral range, it is not possible to retrieve direct information on the isomerization QY from this measurement.

Compound **2**, on the contrary, has a low isomerization QY in all solvents.[30] In this case, the excited state decays very fast, in about 2 ps, as noticed from the decay of the ESA band. It has been previously suggested[30] that the presence of the OMe substituent enhances the conjugation between the hydrazone nitrogen and the rotor moiety, imparting a partial single bond character to the imine C=N bond. This is confirmed by computations, showing that in the ground state of the *Z* isomer, the C=N bond is longer for compound **2** in comparison with the other two molecules (computed bond distances are: 1.315 Å (C1), 1.326 Å (C2); 1.319 Å (C3).) Furthermore, assignment of the FTIR bands also points in this direction (see discussion of Fig. 5). As demonstrated from the rapid excited state deactivation, the presence of a relatively high number of delocalized modes possibly increases the rate of non-radiative recombination, at the expenses of photoinduced isomerization. At the ground state, easier rotation around the C=N bond contributes to decrease the $Z \rightarrow E$ isomerization QY, facilitating the thermal *E* to *Z* isomerization.

Finally, for compound **3**, which shows appreciable florescence in the *Z* form, we observe a recovery of the SE band within 5 ps, together with the rise of a new positive signal, centered at about 515 nm. We interpret this evolution in terms of depletion of the emissive *Z* population through photo-isomerization towards the non-emissive *E* form.

Successively, a further decrease of the ESA band peaked at 670 nm is noticed, accompanied by a partial decay of the bleaching signal, occurring in 80 ps. This evolution can be ascribed to a structural relaxation of the molecules that have reached the ground state upon photo-isomerization. It is known that this sample has a photo-isomerization QY of about 46% in TOL and that the *E* isomer is barely fluorescent.[30] The intensity of the GSB on the long timescale, which is almost half of that observed soon after excitation, and the observed decrease of SE, confirm that almost half of the excited state population undergoes isomerization towards the non-emissive *E* form. The non-isomerized population reverts to the *Z* ground state on a longer timescale mostly through fluorescence emission.

Solvent polarity greatly influences the excited state evolution of the compounds, as shown by inspecting the EADS obtained analysing the transient data recorded in ACN, reported in Fig. 7.

A first observation is that the excited state lifetimes and the appearance of the transient spectra of both sample **1** and **3** are different as compared to the previously analysed nonpolar solvent. The lifetime of sample **3** is particularly affected by polarity, being reduced by almost an order of magnitude in acetonitrile with respect to toluene (see also Fig. S6).

More specifically, for compound **1** the initial EADS in ACN presents a broad, intense ESA band spanning from 430 to 600 nm, appearing as a double peaked band for the presence of a hole at 500 nm, assigned to the superimposed contribution of the SE band of the *Z* isomer. The transient spectrum evolves very rapidly: the deep at 500 nm recovers and is replaced by a broad positive band, while a different negative band, still assigned as a SE, rises at 600 nm.

The evolution of the ESA band, which significantly changes in shape in about 0.8 ps, and the appearance of the SE band peaked at 600 nm, imply that a different excited state is

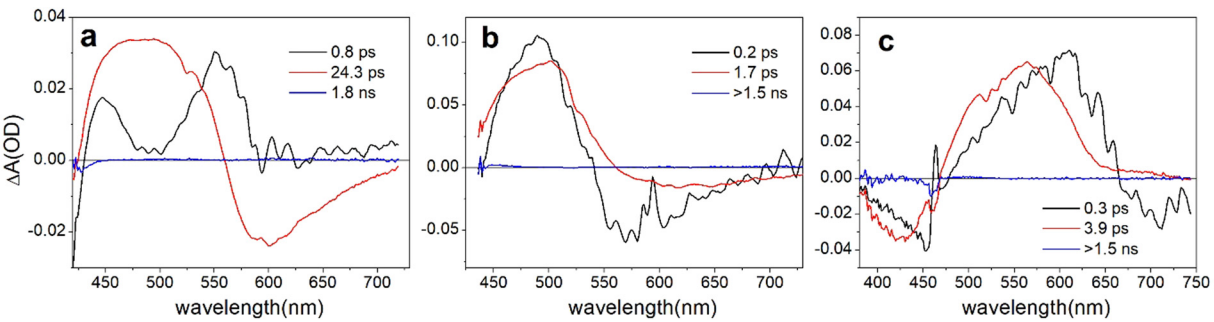

Fig. 7 EADS obtained from global analysis of the transient data recorded by exciting the *Z* isomer of compound (a) **1**; (b) **2**; (c) **3** in ACN.

populated on this fast timescale. Quite recently, Mravec *et al.*[56] reported the transient absorption spectra of hydrazone compounds showing some similarities with those studied in this work and they interpreted their measurements based on DFT computations. The authors assigned the early time component, which appears very similar to that recorded for compound **1** in ACN, to the absorption of the Frank–Condon minimum of the S_1 state of the *Z* isomer. On the following ultrafast timescale, they notice the appearance of a new red shifted SE band, assigned to the emission of a second minimum of the *Z* potential energy surface, located close to a conical intersection (CI) leading to isomerization. According to their calculations in this minimum the sample has a distorted geometry and presents an electronic distribution typical for a CT state, giving rise to the observed red shifted emission.

The spectral evolution observed for compound **1** in ACN indicates similar excited state dynamics, implying that within 0.8 ps a solvent driven relaxation shifts the excited state population from the FC state towards a lower energy state with CT character, responsible for the SE signal peaked at 600 nm. On the following 24 ps timescale (evolution from red to blue EADS), the transient signal decays almost completely, and the system relaxes towards the ground state of the *Z* isomer through internal conversion. The addition of the third long time constant improves the fit, although the very small residual signal observed at the long timescale most likely arises from baseline fluctuations, indicating that minimal (or no) isomerization is observed in ACN.

For compound **2**, solvent polarity does not significantly influence the excited state dynamics, that is very rapid in all solvents, suggesting the absence of CT character.

For compound **3** on the contrary, the excited state lifetime is greatly reduced in polar media. The 520 nm SE band observed in TOL is not noticed in ACN, where instead a red-shifted SE band peaked at 700 nm appears at early times, partially covered by a broad ESA band. The transient spectra decay quite rapidly, in about 4 ps, leaving almost no residual signal on the longer timescale. Similar dynamics is also observed in solvent with medium polarity, such as DCM (see Fig. S6).

The fast spectral evolution observed in polar and moderately polar solvents is indicative for solvent induced relaxation of the excited state, that, as shown by computations, has a CT nature for this molecule. The almost complete decay of the transient signal in polar media on a timescale of <20 ps and the absence of a long living product signal implies that isomerization is greatly suppressed as compared to TOL and the excited state population returns to the ground state mostly by internal conversion. Additional details about transient absorption measurements can be found in SI, where data recorded in DCM for the three compounds are discussed (discussion of Fig. S3–S6).

Transient IR spectroscopy

To gain further structural insights in the photo-isomerization process, we also measured the transient IR spectra of the compounds, using an excitation wavelength of 400 nm for compounds **1** and **2**, and 470 nm for compound **3**. The transient IR spectra of compounds **1** and **2**, measured in both DCM and ACN are reported in the SI (Fig. S16–S21). The transient IR spectra of compound **3** have been recorded in DCM and cyclohexane (Fig. 8). The latter solvent has been selected as a non-polar medium, being toluene is not suitable for IR measurements. The behaviour of compound **3** in toluene and cyclohexane is comparable (Fig. S22), although visible transient absorption measurements indicate that photo-isomerization occurs on a slightly longer timescale in cyclohexane compared to TOL (Fig. S23).

Fig. 8 shows the EADS obtained from global analysis of the transient IR data measured in the two solvents (more data are reported in SI). The spectral changes observed over time in DCM are quite notable. At short pump probe delays (black line in Fig. 9a) a several broad positive ESA signals are noticed, together with bleaching bands, corresponding to the ground modes registered in the FTIR spectrum. In particular, negative signals are noted at 1595, 1530 and 1504 cm^{-1}. Based on the assigned FTIR spectrum, the former is associated with the aromatic C=C stretching, and the latter two signals are associated with delocalized modes involving the C=N and N–N stretching, besides the N–H bending. The spectrum evolves very rapidly towards the second EADS, because of a fast (possibly electronic) excited state relaxation process: we observe a compensation of intensities between the negative bands which become more intense, and the positive bands that decrease in intensity and become narrower. A new bleaching signal at

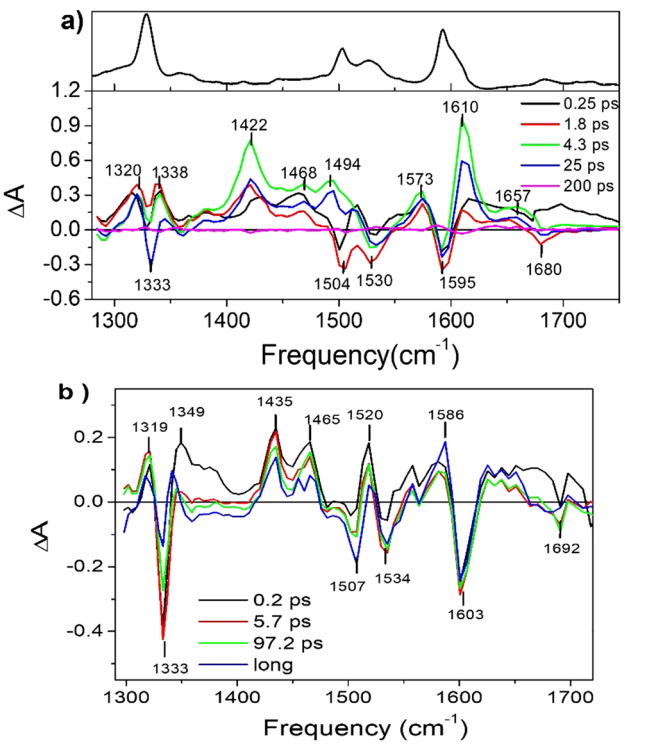

Fig. 8 EADS obtained from global analysis of the transient IR data recorded by exciting the *Z* isomer of compound **3** in (a) DCM and (b) cyclohexane. The FTIR spectrum of the compound measured in DCM is reported on top of panel (a).

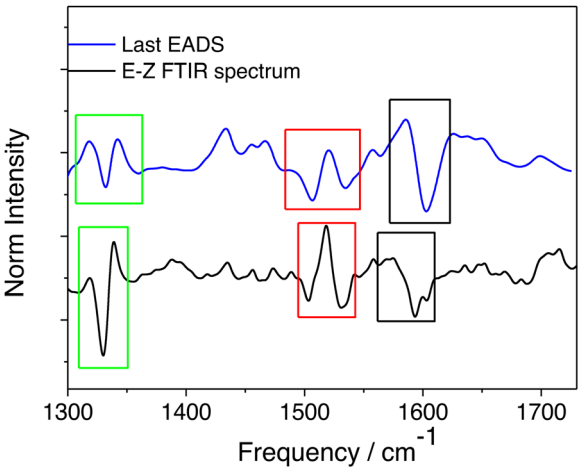

Fig. 9 Comparison between the final EADS obtained from global analysis of the transient IR data in cyclohexane (blue line) and the experimental *E*–*Z* FTIR difference spectrum (measured in DCM because of higher solubility) for compound **3**. The regions discussed in the text are highlighted with black, red, and green boxes.

1680 cm^{-1}, assigned to the C=O stretching, becomes visible in the second EADS. The transient spectrum significantly evolves within 1.8 ps; the intensity of several positive signals, such as those at 1657, 1610 and 1422 cm^{-1}, significantly increases and a new positive band develops at 1494 cm^{-1}. This evolution strongly suggests that an important structural modification occurs on this timescale. Although occurring on slightly different timescales, the spectral changes observed in the IR measurements, which are performed using a concentrated sample, could be related to the evolution observed on the short timescale in the visible transient absorption spectra, leading to the appearance of a red-shifted SE (Fig. 7), and interpreted as a solvent driven relaxation process increasing the CT character of the excited state. Additionally, the transient IR measurements strongly suggest that structural distortions occur in <5 ps, which would drive the molecule towards isomerization[57] through rotation around the central C=N bond, accompanied by H-bond breaking. This process results in an increased electron density localization on the C=O mode, whose frequency is expected to upshift and a decreased electron density on the and C=N, which should instead down-shift at the excited state. Based on these considerations, we can tentatively assign the intense positive band observed at 1610 cm^{-1} in the third EADS in DCM (green line in Fig. 8a) to the upshifted aromatic absorption (this mode absorbs at 1595 cm^{-1} in the *Z* ground state) and the 1468–1494 cm^{-1} positive bands to modes bearing contribution from the downshifted C=N stretching (contributing to the double negative band at 1504–1530 cm^{-1} at the ground state). The interpretation of the positive peaks in the lower frequency region is less evident. Based on computations, the vibrational bands in this region are mostly assigned to modes delocalized over the central part of the molecule, with low intensity at the ground state. These bands could gain oscillator strength in the excited state. The transient IR spectrum does not undergo notable evolution on the following 4.3 ps timescale, except for a general decrease in intensity of the signal and small blue shifts of the positive bands, suggesting excited state relaxation. The transient signal recovers almost completely in about 25 ps, leaving very small residuals, thus confirming, as also observed in the visible, that the excited state mostly relaxes by internal conversion without an appreciable accumulation of the *E* isomer, although undergoing structural distortions that would promote isomerization.

When measurements are repeated in the non-polar cyclohexane, the relaxation dynamics are quite different, as already noticed in the visible pump–probe spectra. In cyclohexane, after light absorption, the excited state undergoes a fast, possibly electronic relaxation, occurring in about 200 fs, evidenced by the decay of several ESA bands in the 1350–1400 cm^{-1} region (Fig. 8b). The transient spectra registered in this solvent can be somehow compared to those in DCM, although spectral evolution is minor in this case. A double peaked positive band is observed at 1435–1465 cm^{-1} possibly associated with downshifted modes delocalized over the central part of the molecule in the excited state, with possible contribution from the C=N stretching. Two additional positive peaks are observed at 1520 and 1582 cm^{-1} which, in agreement with previous discussions, should reflect the frequency shifts of the aromatic stator and rotor stretching modes. All the ESA bands slightly decrease in intensity in the investigated time interval, except for the band at 1586 cm^{-1} which experiences a slight increase in intensity in about 97 ps (evolution from green to blue-EADS). The rise of this band, which can be assigned to the upshifted aromatic stretching, similar to what was observed for the band at 1610 cm^{-1} in DCM, could signal the occurrence of isomerization. It is worth noting that from visible pump–probe measurements, spectral changes signalling isomerization are observed to occur on a similar timescale (see Fig. S23).

Contrary to what is observed in DCM, in cyclohexane the transient signal does not decay on the investigated timescale: in this solvent, photo-isomerization occurs with a good QY and the non-isomerized population reverts to the ground state by fluorescence emission, as similar to TOL. Based on these considerations, the long-lived EADS, that should reflect the *E*–*Z* IR difference spectrum, has been compared to the FTIR *E*–*Z* difference spectrum obtained by irradiating the *Z* sample towards the PSS, see Fig. 9.

As noted from Fig. 9, the agreement between the long-lived EADS and the FTIR difference spectrum is good: both difference spectra present a negative/positive signal at *ca.* 1600/1585 cm^{-1} and similar differential patterns in the 1500–1525 and 1300–1325 cm^{-1} regions (marked with coloured rectangles in Fig. 9). Further support to these conclusions is given by the analysis of the computed frequency changes expected between the *Z* and *E* isomers, confirming that upon photo-isomerization the C=O and aromatic C=C modes upshift in frequency (Fig. S17). It is finally worth noting that the transient IR measurements performed for compound **1** in DCM (Fig. S14) also show the rise of a positive band at about 1590 cm^{-1} on a timescale of a few picoseconds, and the corresponding build-up of a red-shifted stimulated emission in the visible transient absorption spectra,

occurring on the same timescale (see Fig. 5). These spectral changes consistently indicate the occurrence of structural distortions preparing the sample to isomerize. For this compound, the IR data in DCM indicate the formation of a very small amount of photoproduct (see Fig. S17, particularly the long living EADS and kinetic traces), suggesting that although the photo-isomerization QY decreases in DCM as compared to TOL, this excited state deactivation pathway is not completely suppressed.

Coming back to compound **3**, transient absorption measurements both in the visible and IR, consistently suggest that in polar solvents fast recovery towards the ground state through internal conversion prevails over photo-isomerization, while in non-polar solvents the internal conversion rate decreases, favouring isomerization. Finally, in non-polar media the overall excited state lifetime increases, and the non-isomerized population reverts to the ground state emitting fluorescence.

Conclusions

Our combined experimental and theoretical studies allowed us to derive new information about the influence of the solvent and different EWG or EDG substituents on the excited state behaviour of bistable hydrazones. Both computations and transient absorption measurements confirm that the presence of an EDG group on the stator phenyl ring increases the conjugation in the molecule, imparting partial single bond character to the central C=N bond, as previously suggested.[30] This behaviour is exemplified by compound **2**, which indeed presents a highly reduced photo-isomerization QY and a rapid excited state deactivation, occurring through internal conversion, facilitated by the ease of forward and back rotation around the central bond. In the case of compounds **1** and **3** the excited state lifetime is greatly affected by solvent polarity. The analysis of the transient data suggests that in polar solvents these molecules undergo notable structural distortions on a fast, picosecond timescale, but mostly revert to the ground state by internal conversion, without appreciable photoproduct accumulation. Indeed, solvent polarity lowers the excited state energy, which has a CT character and is stabilized through a fast solvation-induced relaxation. Our data suggest that the rate of different non-radiative deactivation channels, mostly connected to vibrational relaxation, increases in polar environments competing with isomerization and largely leading to its suppression. In non-polar solvents, photo-isomerization is accessible for both compound **1** and **3**. For compound **3**, the excited state lifetime is longer in toluene as compared to DCM or ACN and the fraction of non-isomerized population reverts to the ground state by fluorescence emission. Our analysis shows that while on one hand the addition of EDG and EWG substituents is useful in red-shifting the absorption spectra of the hydrazone photoswitches, it also makes the photo-isomerization QY quite sensitive to the polarity of the medium, which should be considered in view of possible biological applications. Overall, our study contributes to the understanding of key structural factors that influence the photoswitching activity of the studied hydrazones and can help in designing new switchable systems with improved properties.

Conflicts of interest

There are no conflicts of interest to declare.

Data availability

The data supporting this article have been included as part of the SI.

Additional steady state and time resolved data, and computational analysis. See DOI: **https://doi.org/10.1039/d5cp01160d**

Acknowledgements

I. A. is thankful for generous support from the NSF MSN program (CHE-2304983). Computations were performed, in part, on the Vermont Advanced Computing Center.

References

1 B. L. Feringa and W. R. Brown, in *Molecular Switches*, ed. B. L. Feringa and W. R. Brown, Wiley-VCH, Weinheim, Germany, 2011.
2 R. Klajn, J. F. Stoddart and B. A. Grzybowski, *Chem. Soc. Rev.*, 2010, **39**, 2203–2237.
3 B. K. Pathem, S. A. Claridge, Y. B. Zheng and P. S. Weiss, *Annu. Rev. Phys. Chem.*, 2013, **64**, 605–630.
4 D. Gust, T. A. Moore and A. L. Moore, *Chem. Commun.*, 2006, 1169–1178.
5 A. Lennartson, A. Roffey and K. Moth-Poulsen, *Tetrahedron Lett.*, 2015, **56**, 1457–1465.
6 J. Otsuki, M. Tsujino, T. Iizaki, K. Araki, M. Seno, K. Takatera and T. Watanabe, *J. Am. Chem. Soc.*, 1997, **119**, 7895–7896.
7 V. Blanco, D. A. Leigh and V. Marcos, *Chem. Soc. Rev.*, 2015, **44**, 5341–5370.
8 T. Senthilkumar, L. Zhou, Q. Gu, L. Liu, F. Lv and S. Wang, *Angew. Chem., Int. Ed.*, 2018, **57**, 13114–13119.
9 J.-J. Yu, Z.-Q. Cao, Q. Zhang, S. Yang, D.-H. Qu and H. Tian, *Chem. Commun.*, 2016, **52**, 12056–12059.
10 B. L. Feringa, *Angew. Chem., Int. Ed.*, 2017, **56**, 11060–11078.
11 S. Kassem, T. van Leeuwen, A. S. Lubbe, M. R. Wilson, B. L. Feringa and D. A. Leigh, *Chem. Soc. Rev.*, 2017, **46**, 2592–2621.
12 J.-P. Sauvage, *Angew. Chem., Int. Ed.*, 2017, **56**, 11080–11093.
13 J. F. Stoddart, *Angew. Chem., Int. Ed.*, 2017, **56**, 11094–11125.
14 S. P. Laptenok, A. A. Gil, C. R. Hall, A. Lukacs, J. N. Iuliano, G. A. Jones, G. M. Greetham, P. Donaldson, A. Miyawaki, P. J. Tonge and S. R. Meech, *Nat. Chem.*, 2018, **10**, 845–852.
15 X. Zhang, M. Zhang, D. Li, W. He, J. Peng, E. Betzig and P. Xu, *Proc. Natl. Acad. Sci. U. S. A.*, 2016, **113**, 10364–10369.
16 K. Hull, J. Morstein and D. Trauner, *Chem. Rev.*, 2018, **118**, 10710–10747.

17 J. Broichhagen, J. A. Frank and D. Trauner, *Acc. Chem. Res.*, 2015, **48**, 1947–1960.
18 M. M. Lerch, M. J. Hansen, G. M. van Dam, W. Szymanski and B. L. Feringa, *Angew. Chem., Int. Ed.*, 2016, **55**, 10978–10999.
19 W. A. Velema, W. Szymanski and B. L. Feringa, *J. Am. Chem. Soc.*, 2014, **136**, 2178–2191.
20 H. M. D. Bandara and S. C. Burdette, *Chem. Soc. Rev.*, 2012, **41**, 1809–1825.
21 M. Irie, T. Fukaminato, K. Matsuda and S. Kobatake, *Chem. Rev.*, 2014, **114**, 12174–12277.
22 R. Klajn, *Chem. Soc. Rev.*, 2014, **43**, 148–184.
23 B. Shao and I. Aprahamian, *Chem*, 2020, **6**, 2162–2173.
24 M. J. Moran, M. Magrini, D. M. Walba and I. Aprahamian, *J. Am. Chem. Soc.*, 2018, **140**, 13623–13627.
25 A. Ryabchun, Q. Li, F. Lancia, I. Aprahamian and N. Katsonis, *J. Am. Chem. Soc.*, 2019, **141**, 1196–1200.
26 X. Guo, B. Shao, S. Zhou, I. Aprahamian and Z. Chen, *Chem. Sci.*, 2020, **11**, 3016–3021.
27 S. Yang, D. Larsen, M. Pellegrini, S. Meier, D. F. Mierke, S. R. Beeren and I. Aprahamian, *Chem*, 2021, **7**, 2190–2200.
28 R. Liang, J. Samanta, B. Shao, M. Zhang, R. J. Staples, A. D. Chen, M. Tang, Y. Wu, I. Aprahamian and C. Ke, *Angew. Chem., Int. Ed.*, 2021, **60**, 23176–23181.
29 B. Shao, M. Baroncini, H. Qian, L. Bussotti, M. Di Donato, A. Credi and I. Aprahamian, *J. Am. Chem. Soc.*, 2018, **140**, 12323–12327.
30 B. Shao, H. Qian, Q. Li and I. Aprahamian, *J. Am. Chem. Soc.*, 2019, **141**, 8364–8371.
31 G. Wang, Y. Li, T. Song, C. Shang, J. Yang, M. Lily, Y. Fang and F. Liu, *J. Phys. Chem. A*, 2020, **124**, 6411–6419.
32 I. H. M. van Stokkum, D. S. Larsen and R. van Grondelle, *Biochim. Biophys. Acta, Bioenerg.*, 2004, **1657**, 82–104.
33 E. R. Henry and J. Hofrichter, *Methods in Enzymology*, Academic Press, 1992, vol. 210, pp. 129–192.
34 J. J. Snellenburg, S. Laptenok, R. Seger, K. M. Mullen and I. H. M. van Stokkum, *J. Stat. Softw.*, 2012, **49**, 1–22.
35 M. D. Hanwell, D. E. Curtis, D. C. Lonie, T. Vandermeersch, E. Zurek and G. R. Hutchison, *J. Cheminf.*, 2012, **4**, 17.
36 F. Neese, *Wiley Interdiscip. Rev.: Comput. Mol. Sci.*, 2012, **2**, 73–78.
37 F. Neese, *Wiley Interdiscip. Rev.: Comput. Mol. Sci.*, 2018, **8**, e1327.
38 F. Weigend and R. Ahlrichs, *Phys. Chem. Chem. Phys.*, 2005, **7**, 3297–3305.
39 J. P. Perdew, M. Ernzerhof and K. Burke, *J. Chem. Phys.*, 1996, **105**, 9982–9985.
40 V. Barone and M. Cossi, *J. Phys. Chem. A*, 1998, **102**, 1995–2001.
41 J.-D. Chai and M. Head-Gordon, *Phys. Chem. Chem. Phys.*, 2008, **10**, 6615–6620.
42 F. Neese, *WIREs Comput. Mol. Sci.*, 2022, **12**(5), e1606.
43 W. Humphrey, A. Dalke and K. Schulten, *J. Mol. Graphics*, 1996, **14**, 33–38.
44 J. P. Perdew, K. Burke and M. Ernzerhof, *Phys. Rev. Lett.*, 1996, **77**, 3865–3868.
45 P. J. Stephens, F. J. Devlin, C. F. Chabalowski and M. J. Frisch, *J. Phys. Chem.*, 1994, **98**, 11623–11627.
46 A. D. Becke, *J. Chem. Phys.*, 1993, **98**, 5648–5652.
47 C. Lee, W. Yang and R. G. Parr, *Phys. Rev. B: Condens. Matter Mater. Phys.*, 1988, **37**, 785–789.
48 J.-D. Chai and M. Head-Gordon, *J. Chem. Phys.*, 2008, **128**, 6615–6620.
49 M. Casanova-Páez, M. B. Dardis and L. Goerigk, *J. Chem. Theory Comput.*, 2019, **15**, 4735–4744.
50 T. Le Bahers, C. Adamo and I. Ciofini, *J. Chem. Theory Comput.*, 2011, **7**, 2498–2506.
51 D. J. Tozer, *J. Chem. Phys.*, 2003, **119**, 12697–12699.
52 C. A. Guido, P. Cortona, B. Mennucci and C. Adamo, *J. Chem. Theory Comput.*, 2013, **9**, 3118–3126.
53 F. Plasser, M. Wormit and A. Dreuw, *J. Chem. Phys.*, 2014, **141**, 024106.
54 F. Plasser, *J. Chem. Phys.*, 2020, **152**, 084108.
55 F. Plasser and H. Lischka, *J. Chem. Theory Comput.*, 2012, **8**, 2777–2789.
56 B. Mravec, S. Budzàk, M. Medved', L. F. Pasteka, C. Slavov, T. Sabmannshausen, J. Wachtveitl, J. Kozisek, L. Hegedusová, J. Filo and M. Cigan, *J. Org. Chem.*, 2021, **86**, 11633–11646.
57 S. Sasaki, G. P. C. Drummen and G.-I. Konishi, *J. Mater. Chem. C*, 2016, **4**, 2731–2743.